METALS AND MATERIALS International, Vol. 11, No. 2 (2005), pp. 141~147

Effect of Cr, Nb, Mn, V, W and Si on High Temperature Oxidation of TiAl Alloys

Dong-Bok Lee*

Department of Advanced Materials Engineering, Sungkyunkwan University,
300 Chunchun-dong, Changan-ku, Suwon 440-746, Korea

Alloys of Ti-(47,51)Al, Ti47Al-4Cr, Ti48Al-2Cr2Nb, Ti47Al-1Mn, Ti39.4Al-10V, Ti48.4Al-1.9W, and Ti43Al-2W0.1Si were oxidized at temperatures between 800 and 1000 °C in air to determine the effect of each alloying element on oxidation behavior. Among the alloys tested, the Ti48.4Al-1.9W alloy displayed the best oxidation resistance, due to the beneficial effects of W, whereas the Ti39.4Al-10V alloy displayed the worst oxidation resistance, due to the formation of volatile V-oxides. Cr was harmful while Nb was beneficial. The oxidation rate of each alloy was not strictly proportional to temperature, because each alloying element had different temperature sensitivity with respect to oxidation rate.

Keywords: TiAl, intermetallics, high temperature oxidation, chromium, niobium, manganese, vanadium, tungsten, silicon

1. INTRODUCTION

Gamma titanium aluminides, whose compositions are generally based on Ti-(45~48) at.%Al to yield a two phase (γ-TiAl+ α_2-Ti_3Al) structure, have attractive properties for high temperature structural applications because of their low density, high melting points, high specific elastic moduli, and high strength at elevated temperatures [1-3]. However, their usage has been limited by poor ductility at room temperature, poor plastic workability even at temperatures above 1000 °C, and insufficient creep and oxidation resistances at high temperatures. The creep and oxidation limits of the titanium aluminides are generally 1000 and 900 °C, respectively [3]. To enhance performance levels, extensive efforts have been made through alloy modifications, process control, and microstructure changes. For example, the additions of (1-3) %(Cr, V, Mn) or 2 %Cr-2 %Nb in two phase gamma compositions yielded improved ductility, due mainly to grain refinement [1-3]. The TiAl-W alloys, meanwhile, were developed for maximum creep resistance [1-3].

Titanium is a strong oxide- and nitride-former, and it has a similar stability in oxygen with Al. Hence, from the surface, (an outer TiO_2 layer)/(an intermediate Al_2O_3 layer)/(an inner (TiO_2, Al_2O_3) mixed layer)/(islands of TiN and/or TiAlN at the scale-matrix interface)/(an oxygen affected zone just below the scale) form on γ-TiAl alloys during oxidation. The oxidation resistance strongly depends on the continuity and denseness of the intermediate Al_2O_3 layer [4,5]. The aim of this study is to comparatively investigate the oxidation behavior of TiAl alloys containing the following alloying elements: Cr, Nb, Mn, V, W and Si. The information obtained here can be used to design better γ-TiAl alloys for higher temperature applications.

*Corresponding author: dlee@yurim.skku.ac.kr

2. EXPERIMENTAL PROCEDURE

The alloys tested in this study are listed in Table 1. After being cut into sizes of 10×5×5 mm^3, the alloys were ground to a 1000 grit finish, ultrasonically cleaned in acetone and methanol, and oxidized at temperatures of 800, 900 and 1000 °C in atmospheric air. The alloys were loaded in an alumina crucible, and oxidized in a thermogravimetric analyzer (TGA). Duplicate runs were carried out to assess the reproducibility of the data. The oxidized specimens were investigated by the use of scanning electron microscopy (SEM), electron probe microanalysis (EPMA), and X-ray diffraction (XRD).

3. RESULTS AND DISCUSSION

3.1. Pure Ti-(47,51) % Al alloys

Fig. 1 shows the oxidation kinetics of the pure Ti-(47,51) Al alloys between 800 and 1000 °C in air, along with those of the other alloys. The pure TiAl alloys oxidized nearly parabolically at 800 and 900 °C, indicating that the overall reaction was diffusion-controlled. The oxidation kinetics were

Table 1. Nominal composition of the prepared alloys

Designation	Chemical composition (at.%)
Ti47Al[(a)]	Ti-47.12Al-0.11O-0.02C-0.01N-0.02H
Ti51Al[(a)]	Ti-50.56Al-0.1O-0.02C-0.01N-0.01H
Ti47Al-4Cr[(a)]	Ti-47.32Al-3.57Cr-0.08O-0.02C-0.01N-0.01H
Ti48Al-2Cr2Nb[(b)]	Ti-48.11Al-2.02Cr-2.0Nb-0.15O-0.03C-0.01N-0.03H
Ti47Al-1Mn[(a)]	Ti-46.79Al-1.18Mn-0.11O-0.02C-0.01N-0.02H
Ti39.4Al-10V[(b)]	in wt.%; Si=0.07, Mn<0.01, Nb=0.01, Fe=0.08, Ni<0.01, Cu<0.01, C=0.016, O=0.10, N=0.005, H=0.0018
Ti48.4Al-1.9W[(c)]	-
Ti43Al-2W0.1Si[(d)]	-

(a) Arc-melted ingots (260 mmϕ×150 mm) were heat treated under vacuum at 1200 °C for 24 h, hot-isostatic-pressed at 1200 °C for 2 h under 1800 atm of argon atmosphere, and forged isothermally at 1150 °C to about 20 mm in thickness with a strain rate of 5×10^{-4} s^{-1}. The matrix consists of γ-grains and α_2/γ lamellas.
(b) Induction skull melted ingot (20 kg) was sectioned to a bar, and hot extruded with a ratio of 7.2 to 16 mmϕ at 1220 °C to eliminate the casting porosity and stabilize the microstructure. The matrix consists of γ-grains, α_2/γ lamellas, and β-Ti. V is the β-Ti stabilizing element.
(c) Ti-48.4Al-1.9W powders having a maximum powder size of 0.5 mm were gas atomized, vacuum encapsulated in stainless steel tubes, and consolidated by hot isostatic pressing at 1250 °C under 200 MPa for 2 h to produce the cylindrical 12 mmψ compacts with >99.9 % full density by Crucible Compaction Metals, Inc. The matrix consists of γ-grains, α_2/γ lamellas and β-Ti. W is the β-Ti stabilizing element.
(d) Vacuum cast to 9 mmϕ cylindrical bars in the form of cast bars approximately 19 mm in diameter and 280 mm in length by Flowserve, Dayton, OH, USA. The matrix consists of γ-grains, α_2/γ lamellas and β-Ti.

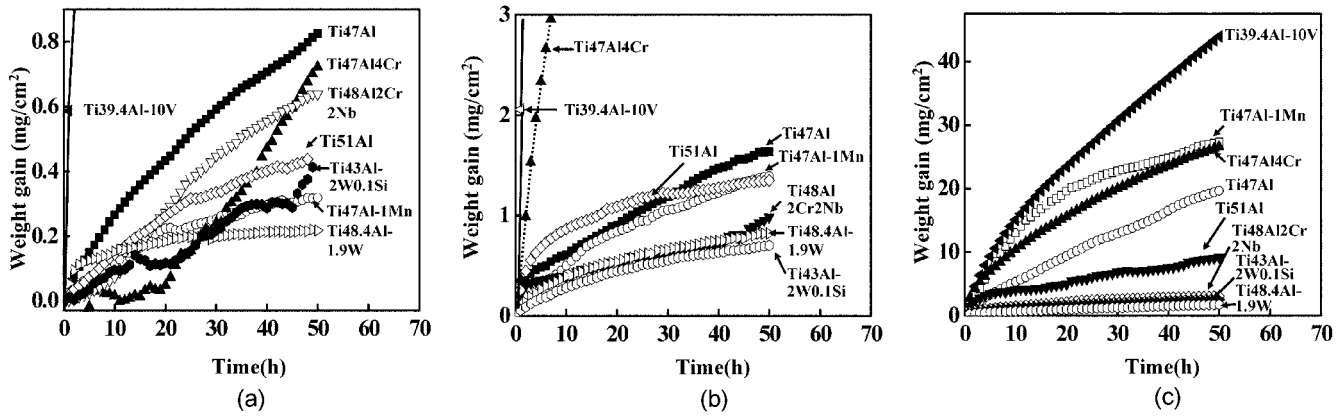

Fig. 1. Weight change vs. time curves of TiAl alloys during oxidation at (a) 800 °C, (b) 900 °C, and (c) 1000 °C in air.

initially parabolic but became linear after a few hours at 1000 °C, indicating that the reaction was rate-controlled in the later stage of oxidation. Ti-51Al displayed better oxidation resistance than Ti-47Al, due to the larger amount of Al.

Fig. 2 shows typical EPMA analytical results of the pure TiAl alloy after oxidation. Consistent with the general understanding, an outer TiO_2 layer, an intermediate Al_2O_3 layer and an inner (TiO_2+Al_2O_3) mixed layer were observed. The Al_2O_3 layer formed was generally discontinuous and diffuse. The oxide scale was partially detached from the matrix. Though the nitrogen profile is uncertain because the N-K_α line overlaps with the Ti-L line, nitrogen from the atmosphere appeared to be present below the outer TiO_2 layer. The formation of TiN and/or TiAlN nitrides, which later oxidize to TiO_2, harmfully prevents the establishment of a continuous Al_2O_3 layer on γ-TiAl [4]. Generally, the oxide scales formed at 800 °C were thin and compact, whereas those formed at 1000 °C were thick and highly nonadherent.

3.2. Ti47Al-4Cr alloys

As shown in Fig. 1, the Ti47Al-4Cr alloy oxidized quite slowly for up to 18 h, but later oxidized almost linearly at 800 °C. By increasing the oxidation temperature, the alloy oxidized rapidly owing to the increased diffusion and reaction rates. Fast growing, nonstoichiometric TiO_2 is an n-type semiconductor. Addition of elements of lower valencies than Ti^{4+} increases the concentration and mobility of defects in TiO_2, while addition of elements of higher valencies than Ti^{4+} reduces the population of mobile defects in TiO_2 to maintain electroneutrality. Hence, Cr, which oxidizes to Cr^{+3}, adversely accelerates the oxidation rates via a doping effect [6,7].

In the XRD pattern of the oxidized specimen shown in Fig. 3(a), strong TiO_2 and weak α-Al_2O_3 peaks are recognizable. γ-TiAl matrix peaks are also seen due to the small extent of oxidation at 800 °C. At higher oxidation temperatures, the nonadherent, thick oxide layer cracked and delaminated easily. In Figs. 3(b) and (c), an outer TiO_2 layer, an

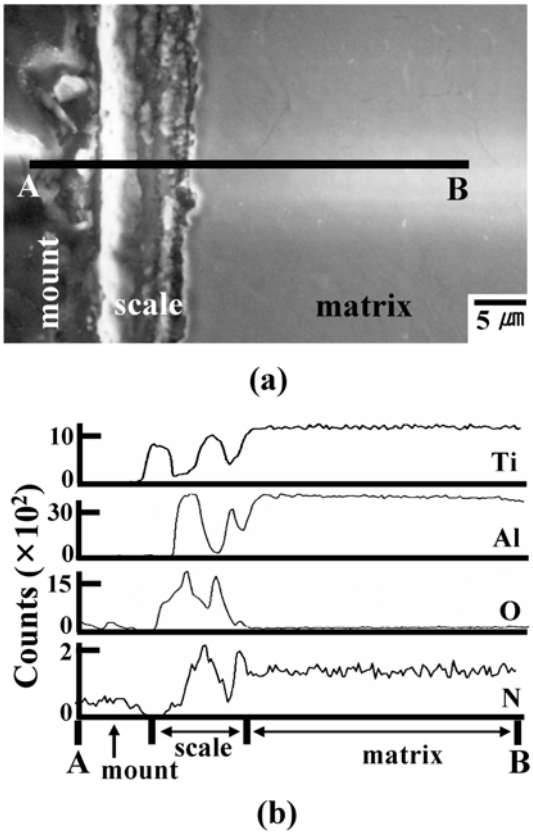

Fig. 2. Ti-51Al after oxidation at 900 °C for 50 h: (a) EPMA cross-sectional image and (b) EPMA line profiles of (a).

intermediate Al_2O_3-rich layer, and an inner (TiO_2+Al_2O_3) mixed layer were observed. The elemental profiles of Ti, Al, O, and N shown in Fig. 3(c) are similar to those of pure TiAl alloys shown in Fig. 2(b). Since Cr is more noble than Ti and Al, it tends to be progressively expelled from growing oxide scales, resulting in the accumulation of Cr around the oxide-matrix interface [7]. The Ti47Al-4Cr alloy displayed poorer oxidation resistance than the pure TiAl alloys.

3.3. Ti48Al-2Cr2Nb alloys

As shown in Fig. 1, at 800 °C, Ti48Al-2Cr2Nb followed a sigmoid oxidation curve, being oxidized slowly, linearly, and parabolically as the reaction progressed. The alloy oxidized slightly faster than Ti51Al at 800 °C, but slower at 900 and 1000 °C. The amount of spalled oxide scales was small in Ti48Al-2Cr2Nb. Its oxidation rate was advantageously less sensitive to the temperature than Ti51Al. Niobium, which oxidizes to Nb^{+5}, decreases the TiO_2-rich scale growth via a doping effect, and reduces the growth stresses, thereby improving the scale adherence [5]. Thus, with the addition of Nb, the harmful doping effect of Cr was suppressed. The oxidation resistance of Ti48Al-2Cr2Nb was better than that of Ti-(47,51)Al and Ti47Al-4Cr.

A typical EPMA image and the elemental line profiles of

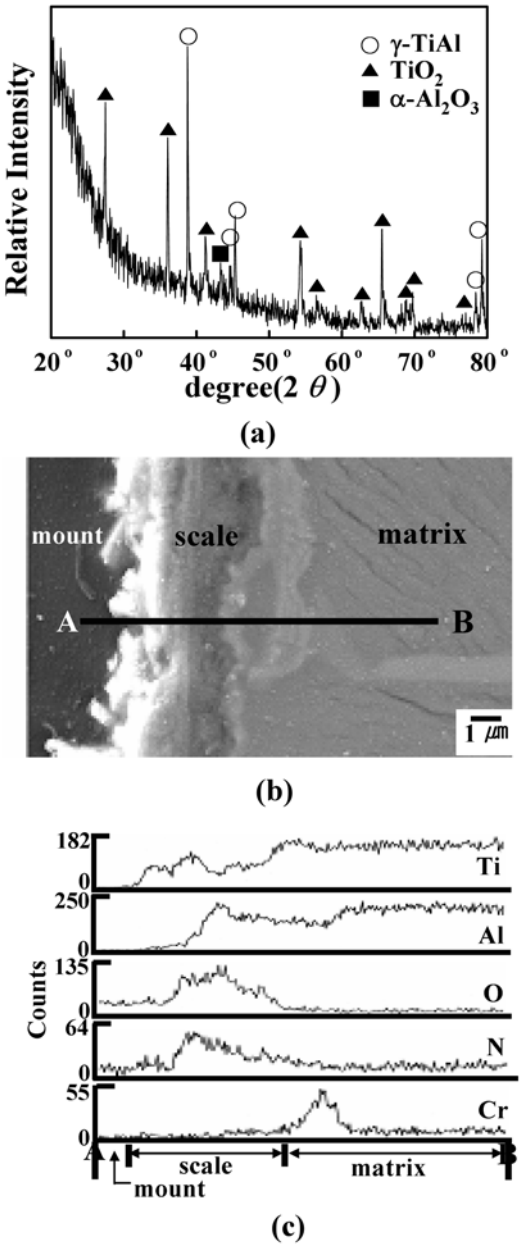

Fig. 3. Ti47Al-4Cr after oxidation at 800 °C for 50 h: (a) XRD pattern, (b) SEM cross-sectional image, and (c) EDS line profiles of (b).

the oxidized specimen are shown in Fig. 4. The characteristic triple-layered oxide scale formed on Ti48Al-2Cr2Nb. The elemental profiles of Ti, Al, O, N, and Cr shown in Fig. 4(b) are similar to those of Ti47Al-4Cr shown in Fig. 3(c). Nitrogen from the atmosphere is present mainly below the intermediate Al_2O_3-rich layer, likely in the form of TiN or TiAlN [4]. The ions of Cr and Nb, whose oxides were not detected from XRD owing to their dissolution in the oxide scale, were mainly enriched around the scale-matrix interface. The noble elements of Cr and Nb, when compared to Ti and Al, tended to be expelled from the growing oxide scale.

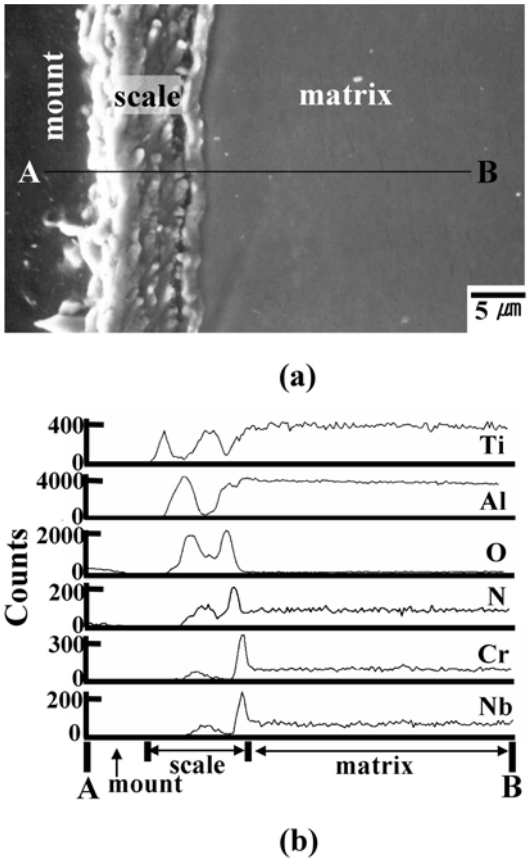

Fig. 4. Ti48Al-2Cr2Nb after oxidation at 900 °C for 40 h: (a) EPMA cross-sectional image and (b) EPMA line profiles of (a).

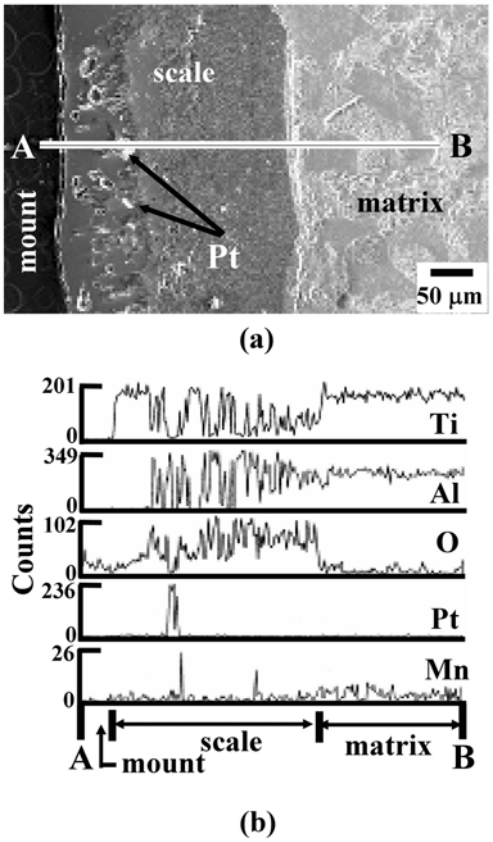

Fig. 5. Ti47Al-1Mn after oxidation at 1000 °C for 15 h: (a) SEM cross-sectional image and (b) EDS line profiles of (a).

3.4. Ti47Al-1Mn alloys

From Fig. 1, it is seen that the Ti47Al-1Mn alloy oxidizes slowly, according to the parabolic rate law at 800 °C. The alloy oxidizes moderately at 900 °C, but oxidizes rapidly at 1000 °C. When compared to Ti(47,51)Al, the oxidation resistance of Ti47Al-1Mn is superior at 800 °C, similar at 900 °C, but poorer at 1000 °C. This variation is attributed to the different temperature sensitivity of the oxidation rate. Mn improved the scale adherence to a certain degree. XRD tests indicated that the major phase of oxides formed was TiO_2, while Al_2O_3 accounted for the minor phase. The oxides of Mn, i.e., $MnTiO_3$ [8-10] and Mn_2O_3 [11] were vaguely detected, because Mn was mostly dissolved in the oxide scale. Also, weak diffraction patterns of TiN and Ti_2AlN, which are known to exist at the scale-matrix interface [12], are frequently detected [13].

Fig. 5 shows the typical cross-sectional EPMA image of the oxide scale and elemental distributions in the oxidized Ti47Al-1Mn alloy. Since the oxidation resistance decreased sharply at 1000 °C, oxidation at 1000 °C for 15 h led to the formation of a quite thick scale. The outer, semi-protective TiO_2 layer had many micropores. The intermediate Al_2O_3 barrier layer was not distinct. The inner (TiO_2+Al_2O_3) mixed layer consisted of alternating TiO_2-rich/Al_2O_3-rich areas. The dissolution of Mn^{2+} or Mn^{3+} in the oxide scale having lower valencies than Ti^{4+} would increase the growth rate of nonstoichiometric TiO_2 by increasing the concentration of interstitial Ti ions and oxygen vacancy to maintain electroneutrality. Hence, Mn decreased the oxidation resistance especially at 1000 °C, because the harmful doping effect was dominant.

3.5. Ti39.4Al-10V alloys

Herold-Schimidt *et al*. [14] previously reported that 1 %V additions to Ti-(40, 48)Al did not significantly change the oxidation resistance and the mechanism at 900 °C. Kekare *et al*. [15] explained that the doping of 2.2 %V having a valence of +5 beneficially improved the oxidation resistance of Ti48Al by annihilating oxygen vacancies in TiO_2 at 982 °C. Shida *et al*. [9,16] performed oxidation studies at 900 °C on Ti48Al-(0.36~3.63)V, and found typically thick, multilayered scales, which indicated that V had a harmful effect. They proposed that V might play some role in accelerating TiO_2 growth. To determine the role of V during the oxidation of TiAl alloys, a Ti39.4Al-10V alloy having a high concentration of V was investigated in this study.

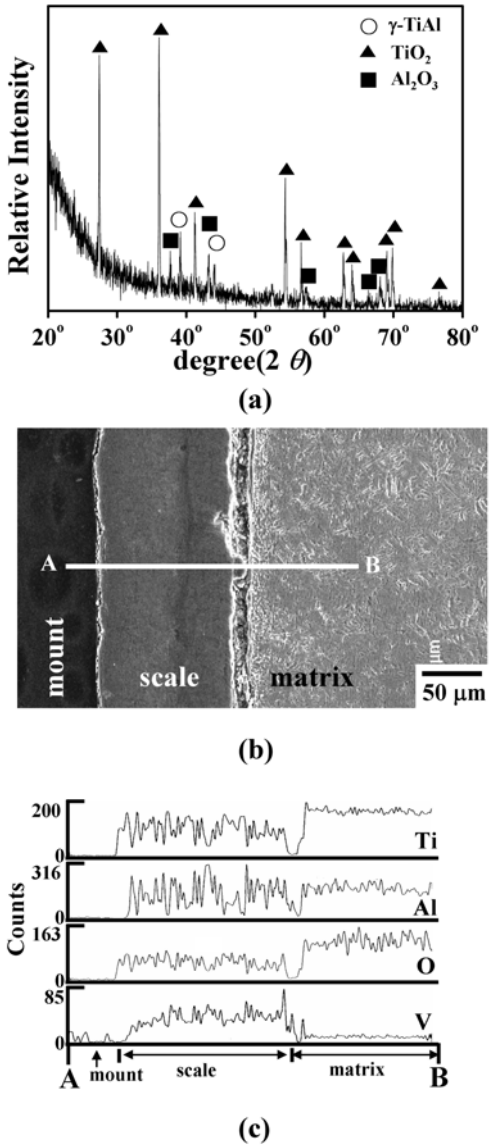

Fig. 6. Ti39.4Al-10V after oxidation at 900 °C for 60 h: (a) XRD pattern, (b) SEM cross-sectional image, and (c) EDS line profiles of (b).

The oxidation kinetics of Ti39.4Al-10V in air are shown in Fig. 1. The alloy oxidized quite rapidly at 800, 900, and 1000 °C. The poor oxidation resistance is attributed to the low Al content and the deleterious effect of V. There are various polymorphic V-oxides, including VO, VO_2, and V_2O_5 that melts at 670 °C. After oxidation, the alumina crucible used to contain the sample was covered with a yellow, thin film in all cases. This film was amorphous, making phase identification using XRD impossible, and it was too thin to identify the composition using EPMA. The yellow film is likely condensed V-oxides.

As shown in Fig. 6(a), only TiO_2, Al_2O_3 and γ-TiAl were detected from XRD on the oxidized samples. The highly volatile V-oxides condensed as an amorphous phase after oxidation during the cooling stage. The corresponding SEM analyses shown in Figs. 6(b) and (c) imply that the outermost TiO_2 layer is thin, the intermediate Al_2O_3 layer is not distinct, and the inner (TiO_2+Al_2O_3) layer is very thick. Vanadium was uniformly distributed throughout the oxide scale. The intermediate Al_2O_3 layer was too thin or discontinuous to protect the alloy from oxidation. Interestingly, the scale image shown in Fig. 6(b) appears dense. In the same manner that the evaporation of water from soil makes the soil dense, evaporation of V-oxides from the scale has made the scale dense. This study indicates that V has a harmful effect on oxidation, as Shida *et al*. have proposed [9,16]. However, the harmful effect is mainly attributed to the formation and subsequent evaporation of V-oxides, which disrupt the formation of a protective scale and deteriorate both the oxidation resistance and the scale adherence significantly.

3.6. Ti48.4Al-1.9W alloys

The oxidation kinetics of the Ti48.4Al-1.9W alloy between 800 and 1000 °C in air are depicted in Fig. 1. The alloy oxidized parabolically up to 1000 °C, with small weight gains. The scale was adherent up to 900 °C, although some scale spalled at 1000 °C. The enhanced scale adherence and the improved oxidation resistance are due to the reduction in the oxygen solubility, the annihilation of oxygen vacancies in TiO_2 by doping W^{+6} [9,16-18], the reduction in the oxygen diffusivity in the alloy, the increment of the Al-diffusivity to form the Al_2O_3 layer, the improvement of scale adherence [19], and compact scale formation [15]. Consistent with previous studies [9,14-19], W was found to be a beneficial element.

A typical X-ray diffraction pattern of the oxidized alloy is shown in Fig. 7(a). Matrix peaks of TiAl, Ti_3Al, and β-Ti as well as nitrides of Ti_2AlN are seen. The oxides are TiO_2 as the major phase, and Al_2O_3 as the minor phase. WO_3 was seldom detected, because of its dissolution in the scale or its small amount. Figs. 7(b) and (c) show typical EPMA results of the oxidized alloy. The etched matrix shows α_2/γ lamellas, γ-colonies (dark area), and β-Ti (whitish islands or rods). The scales consist primarily of an outer TiO_2 layer, an intermediate Al_2O_3 layer, and an inner (TiO_2+Al_2O_3) mixed layer, being analogous to conventional TiAl alloys. The Ti_2AlN layer yielded a nitrogen peak around the scale-matrix interface. A strong W-enrichment was seen at the scale-matrix interface [20]. Tungsten is less oxygen-active and thus has a tendency to be expelled from the growing oxide scale, and thereby can be enriched around the scale-matrix interface. W is proposed as the most effective element in improving oxidation resistance among Cr, Nb, Mn, V and W.

3.7. Ti43Al-2W0.1Si alloys

The oxidation of Ti-(45.0~46.4)Al-(1.1~2.1)W-0.6Si alloys between 600 and 850 °C in air was studied by Tomasi *et al*.

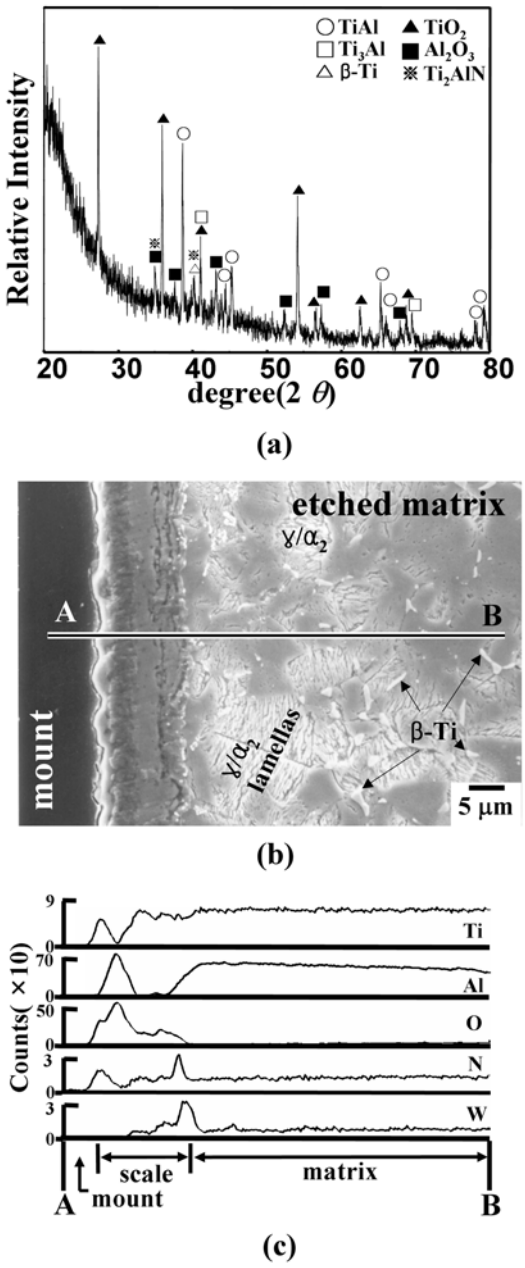

Fig. 7. Ti48.4Al-1.9W after oxidation at 1000 °C for 60 h: (a) XRD pattern, (b) EPMA cross-sectional image, and (c) EPMA line profiles of (b).

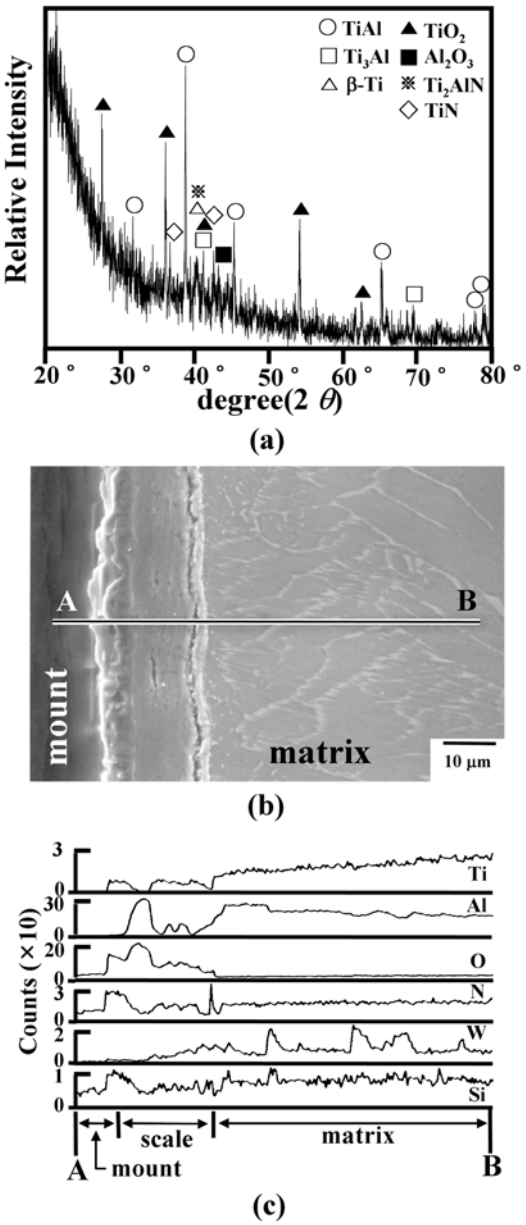

Fig. 8. Ti43Al-2W0.1Si after oxidation at 1000 °C for 60 h: (a) XRD pattern, (b) EPMA cross-sectional image, and (c) EPMA line profiles of (b).

[19,21]. In this study, the Ti43Al-2W0.1Si alloy was oxidation tested between 800 and 1000 °C in air. Like W, Si is a well-known beneficial element in terms of oxidation resistance. The large addition of Si needed to promote protective scale formation however makes the alloy brittle such that it does not exhibit sufficient strength in the target temperature range [5]. The oxidation kinetics of Ti43Al-2W0.1Si are shown in Fig. 1. The alloy oxidizes slowly up to 1000 °C, because of W and Si added.

The XRD pattern of the oxidized Ti43Al-2W0.1Si is shown in Fig. 8(a). This is quite similar to that of the oxidized Ti48.4Al-1.9W shown in Fig. 7(a). Under all the oxidation conditions, TiO_2 was the major oxide, and Al_2O_3 was the minor one. Beside the matrix phases, the weak diffraction patterns of Ti_2AlN and TiN were observable. The Si content in this study was too small to form a separated SiO_2 layer or SiO_2 patches. W-oxides were seldom detected owing to either their dissolution in the (TiO_2, Al_2O_3) oxides or their small amount. WO_3 was detected from XRD in some instances, indicating that a certain amount of WO_3 can be formed. This is evidenced by the abnormal weight gain curve of Ti43Al-2W0.1Si at 800 °C. WO_3 can harmfully disrupt compact scale formation, because of its high vapor pressure. Hence, the addition of a

larger amount of Al is recommended for the TiAl-W base alloys to deter the formation of WO_3. Figs. 8(b) and (c) show typical EPMA results of the oxidized alloy. The oxide scales consisted primarily of an outer TiO_2 layer, an intermediate, distinctive Al_2O_3-rich layer, and an inner mixed layer of (TiO_2+Al_2O_3). Tungsten, being the less active element, tended to be expelled from the outer TiO_2 layer. The active element of Si was present over the whole oxide scale. Ti43Al-2W0.1Si has poorer oxidation resistance than Ti48.4Al-1.9W, due to the decreased amount of Al.

4. CONCLUSION

Alloys of Ti-(47,51)Al, Ti47Al-4Cr, Ti48Al-2Cr2Nb, Ti47Al-1Mn, Ti39.4Al-10V, Ti48.4Al-1.9W, and Ti43Al-2W0.1Si were oxidized between 800 and 1000 ^oC in air. The best oxidation resistance was obtained in Ti48.4Al-1.9W, whereas the worst oxidation resistance was observed in Ti39.4Al-10V. Nb, W, and Si were found to be beneficial, while Cr and V were harmful. Depending on the activity of the alloying element and the extent of oxidation, Cr, Nb, and W were mainly present below the intermediate Al_2O_3 layer. V, Mn, and Si were mainly present throughout the scale. Below the oxide scale, TiN and/or TiAlN were frequently detected.

ACKNOWLEDGMENT

This study was supported by the Korea Science and Engineering Foundation under the ERC project.

REFERENCES

1. Y. W. Kim, *J. Met.* **41**, July, 24 (1989).
2. Y. W. Kim, *J. Met.* **46**, July, 30 (1994).
3. F. H. Froes and C. Suryanarayana, *Physical Metallurgy and Processing of Intermetallic Compounds*, p. 297, Chapman & Hall, Inc., NY (1996).
4. M. P. Brady, W. J. Brindley, J. L. Smialek, and I. E. Locci, *J. Met.* **48**, Nov., 46 (1996).
5. I. C. I. Okafor and R. G. Reddy, *J. Met.* **51**, June, 35 (1999).
6. H. G. Jung, C. H. Oh, and K. Y. Kim, *J. Kor. Inst. Met. & Mater*. **38**, 1053 (2000).
7. J. H. Won, Y. J. Kim, S. W. An, and D. B. Lee, *J. Kor. Inst. Met. & Mater*. **36**, 546 (1996).
8. K. Kasahara, K. Hashimoto, H. Doi, and T. Tsujimoto, *J. Jpn. Inst. Met.* **54,** 948 (1990).
9. Y. Shida and H. Anada, *Oxid. Met*. **45,** 197 (1996).
10. K. Shibue, M. Kumagai, and M. S. Kim, *J. Jpn Inst. Met.* **56,** 1457 (1992).
11. V. A. C. Haanappel, J. D. Sunderkotter, and M. F. Stroosnijder, *Intermetallics* **7**, 529 (1999).
12. S. Becker, A. Rahmel, M. Schorr, and M. Schütze, *Oxid. Met*. **38,** 425 (1992).
13. D. B. Lee, Y. D. Jang, and M. Nakamura, *Mater. Trans*. **43**, 2531 (2002).
14. U. Herold-Schmidt, B. Opolka, and S. Schwantes, *Prakt. Metallogrt*. **30**, 7 (1993)
15. S. A. Kekare and P. B. Aswath, *J. Mater. Sci*. **32**, 2485 (1997).
16. Y. Shida and H. Anada, *Corros. Sci*. **35**, 945 (1993).
17. H. Anada and Y. Shida, *J. Jpn Inst. Met*. **58**, 1036 (1994).
18. Y. Shida and H. Anada, *Mater. Trans. JIM* **35**, 623 (1994).
19. A. Tomasi, C. Noseda, M. Nazmy, and S. Gialanella, *MRS Symp. Proc*. **460**, 225 (1997).
20. W. S. Shim and D. B. Lee*, Met. Mater. -Int*. **9**, 473 (2003).
21. A. Tomasi, S. Gialanella, P. G. Orsini, and M. Nazmy, *MRS Symp. Proc*. **364**, 999 (1995).